Mével, C., Gillis, K.M., Allan, J.F., and Meyer, P.S. (Eds.), 1996
Proceedings of the Ocean Drilling Program, Scientific Results, Vol. 147

23. MAGNETIC FABRICS AND SOURCES OF MAGNETIC SUSCEPTIBILITY IN LOWER CRUSTAL AND UPPER MANTLE ROCKS FROM HESS DEEP[1]

Carl Richter,[2] Paul R. Kelso,[3] and Christopher J. MacLeod[4]

ABSTRACT

We present a magnetic fabric study of mafic and ultramafic rocks recovered at Ocean Drilling Program Sites 894 and 895 from Hess Deep, a tectonic rift in the equatorial East Pacific (2°15′N, 101°30′W). We demonstrate, using thermomagnetic curves and high-field (up to 1.5 T) susceptibility measurements, that the magnetite contributes >95% of magnetic susceptibility of these rocks. Bulk susceptibilities for the Site 894 gabbroic rocks are on average 1.72×10^{-2} and for the Site 895 peridotites 4.29×10^{-2} (SI volume units). The anisotropy of magnetic susceptibility is moderate to high and average k_{max}/k_{min} is 1.15 ($k_{max} \geq k_{int} \geq k_{min}$ are the principal susceptibilities) at Site 894 and 1.11 at Site 895. Because of the pervasive serpentinization and the formation of randomly distributed secondary magnetite, the magnetic fabrics of the Site 895 peridotites show no apparent relationship to structural features. In the foliated gabbroic rocks from Site 894, we observe a close relationship between magmatic flow fabrics (defined by the preferred orientation of plagioclase) and magnetic fabrics: k_{min} is perpendicular to the macroscopic foliation and k_{max} dips steeply within the foliation plane and is parallel to the magmatic mineral lineation. Macroscopically isotropic gabbros yield the same principal susceptibility directions as the foliated gabbros. We interpret magnetic fabrics in these rocks to represent a weakly developed rock fabrics. We argue that the process for the development of the AMS is a distribution anisotropy which is caused by the growth of equant, irregular, or skeletal magnetite grains into a preferredly oriented (by magmatic flow) plagioclase "template." Magnetic fabric data record a mineral preferred orientation with a north–south, East Pacific Rise parallel strike and a near-vertical inclination, and can be interpreted to record the upward flow of melt at the top of an axial magma chamber into the base of an overlying sheeted dike complex.

INTRODUCTION

Sites 894 and 895 of Ocean Drilling Program (ODP) Leg 147 are located in Hess Deep on the eastern flank of the East Pacific Rise (EPR) in the equatorial East Pacific (Fig. 1). The unique position at the tip of a westward-propagating rift between the Cocos and Nazca Plates makes Hess Deep an ideal target to study magnetic properties in a vertical section of lower crustal and upper mantle rocks at a fast spreading (130 mm/yr) oceanic ridge. The western end of the rift valley is situated in approximately 1-Ma-old EPR crust. The drill sites are located on an intrarift ridge in water depths of about 3023 m (Site 894) and about 3820 m (Site 895) in an area that has been geologically mapped by submersibles (Francheteau et al., 1990; Karson et al., 1992).

We discuss the rock magnetic properties of basically two different rock types (peridotites and gabbroic rocks, that are both affected by varying degrees of serpentinization and alteration). Hole 894G was drilled to 154 meters below seafloor (mbsf) and mainly gabbronorites and olivine gabbros were recovered; Hole 895D was drilled to 94 mbsf and mainly harzburgites were recovered. Hole 895E reached 88 mbsf and was drilled mainly through dunites, gabbroic rocks, and harzburgites (Gillis, Mével, Allan, et al., 1993).

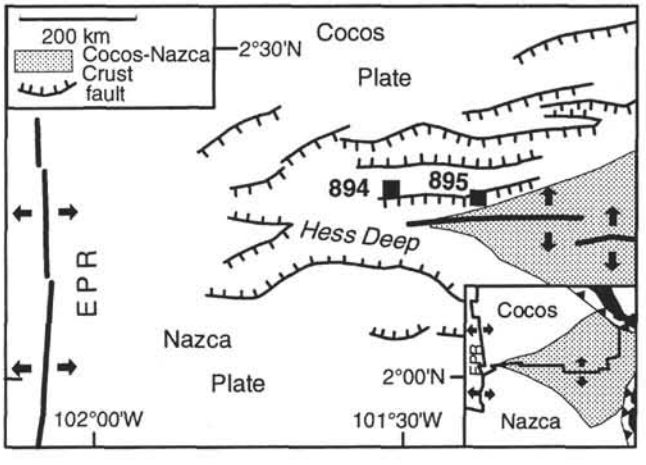

Figure 1. Location of Leg 147 Sites 894 and 895 and generalized tectonic setting of the Hess Deep rift in the equatorial East Pacific (after Lonsdale, 1988) near the junction of the East Pacific Rise (EPR) and the Galapagos spreading center (inset).

The anisotropy of magnetic susceptibility (AMS; reviews by Borradaile, 1988; Tarling and Hrouda, 1993) of most rock-forming minerals (e.g., paramagnetic muscovite, biotite, chlorite) is linked to the crystallographic lattice, that is, the principal susceptibility axes depend on the crystal symmetry (Nye, 1985), parallel to the crystallographic axes (magnetocrystalline anisotropy; e.g., Borradaile and Werner, 1994). This relationship allows the use of magnetic anisotropies as an easy-to-apply proxy for measuring crystallographic preferred orientations (Hrouda and Schulman, 1990; Richter et al., 1993) if it can be demonstrated that the magnetic fabric is due to minerals

[1] Mével, C., Gillis, K.M., Allan, J.F., and Meyer, P.S. (Eds.), 1996. *Proc. ODP, Sci. Results*, 147: College Station, TX (Ocean Drilling Program).

[2] Ocean Drilling Program and Department of Geology and Geophysics, Texas A&M University, 1000 Discovery Drive, College Station, TX 77840, U.S.A.

[3] Institute for Rock Magnetism, University of Minnesota, Minneapolis, MN 55455. (Current address: Lake Superior State University, Sault Sainte Marie, MI 49783, U.S.A.)

[4] Department of Earth Sciences, University of Wales College of Cardiff, P.O. Box 914, Cardiff CF1 3YE, United Kingdom. Formerly at: Institute of Oceanographic Sciences, Brook Road, Wormley, Surrey GU8 5UB, United Kingdom; and Borehole Research, Department of Geology, University of Leicester, Leicester LE1 7RH, United Kingdom. macleod@cardiff.ac.uk

with a magnetocrystalline anisotropy (e.g., Housen and van der Pluijm, 1990). The magnetic anisotropy of ferrimagnetic magnetite is caused by shape anisotropy (Uyeda et al., 1963); that is, for multidomain magnetite, the maximum susceptibility is parallel to the long mineral axis and the minimum susceptibility parallel to the short axis. The magnetic susceptibility of magnetite is many times higher than the susceptibility of paramagnetic minerals and small traces of magnetite can entirely dominate the magnetic susceptibility. Alignment or preferred distribution of (equant) magnetite grains can lead to a distribution anisotropy (Wolff et al., 1989; Hargraves et al., 1991; Stephenson, 1994). AMS data can only be interpreted meaningful if the sources of magnetic susceptibility are known.

The anisotropy of remanence, especially the anisotropy of anhysteretic remanent magnetization (AARM; McCabe et al., 1985; Jackson, 1991), measures the anisotropy of ferro(i)magnetic minerals only. In this technique, an anhysteretic remanent magnetization (ARM) is imparted to a sample using a low steady (bias) magnetic field superimposed on the alternating field of an alternating field (AF) demagnetizer. The resulting ARM is measured and the process is repeated in nine different orientations. If both the AF and the direct current (DC) field are well below the coercivities of hematite, goethite, and fine-grained pyrrhotite, the AARM can only be due to the magnetic anisotropy of magnetite, coarse-grained pyrrhotite, or greigite.

The few studies on the magnetic anisotropy of ultramafic rocks from the oceanic crust (Smith and Banerjee, 1985; MacDonald and Ellwood, 1988; Bina et al., 1990; Bina and Henry, 1990) have shown the existence of relatively strong magnetic anisotropies. Serpentinized peridotites from Hole 670A in the Mid-Atlantic Ridge south of the Kane Fracture Zone show that k_{min} clusters around [010] of olivine (i.e., parallel to the spinel foliation) and k_{max} around the spinel lineation (Bina et al., 1990). This relationship appears to be invalid for highly serpentinized samples. Magnetic fabrics of samples from the Kane Fracture Zone are often related to the high-temperature deformation developed prior to serpentinization: the maximum axes that correspond to the long axes of magnetite particles are parallel to the tectonic lineation, and the minimum axes (perpendicular to the flattening of magnetite particles) are perpendicular to the foliation. Extensively serpentinized samples contain more dispersed secondary pseudo-single-domain magnetite and show little or no relationship between olivine crystallographic preferred orientation (CPO) and magnetic fabric. Wagner et al. (1981) studied the magnetic anisotropy of ophiolitic gabbros from the western Alps. The observed susceptibilities are low (200–578 $\times$ 10^{-6}) and the magnetic fabric is dominated by paramagnetic hornblende and augite minerals. In this case, AMS determines the CPO of the paramagnetic minerals, where k_{min} is parallel to the pole of the foliation plane and k_{max} parallel to the tectonic lineation. Ernst and Baragar (1992) inferred the magma flow pattern and magmatic processes of a huge dike swarm from AMS measurements on mafic igneous rocks which are macroscopically isotropic.

AMS is a very sensitive petrofabric tool, especially in rocks that lack a macroscopic fabric, as is the case in many of the isotropic-looking gabbros recovered at Hess Deep. Using 138 specimens obtained during Leg 147, our goal was to (1) quantify the sources of magnetic susceptibility and the origin of magnetic anisotropy in these mafic and ultramafic rocks, (2) investigate the orientation and shape of induced and remanent magnetic anisotropies, (3) use magnetic anisotropies to characterize the rock fabric, and (4) relate magnetic anisotropies to observed structural features.

EXPERIMENTAL PROCEDURES

Cylindrical specimens (diameter = 2.5 cm, length = 2.2 cm) were drilled from the working half of sampled cores. The anisotropy of low-field magnetic susceptibility (AMS) of the specimens was measured using a KLY-2 Kappabridge (Geofyzika Brno, inducing field = 0.5 mT) on the *JOIDES Resolution* and with a custom-built susceptibility bridge (inducing field = 0.1 and 1.0 mT) at the Institute for Rock Magnetism (IRM) at the University of Minnesota. The CS-2 furnace attachment for the Kappabridge at the IRM was used to determine the temperature dependence of magnetic susceptibility between room temperature and 700°C. For AARM analysis, specimens were first demagnetized using a Schonstedt GSD-1 alternating field (AF) demagnetizer to obtain a baseline measurement that accounts for the remanent magnetizations that the AF demagnetizer did not remove. A DC-powered coil around the AF demagnetizer coil generates a steady magnetic field of 0.05 mT. The ARM was generated over the 0–95 mT field range in nine different orientations. The sample was demagnetized after each step. The AARM tensor was calculated following the method of Girdler (1961). High-field susceptibilities (up to 1.5 T) were determined using the Princeton Applied Research vibrating sample magnetometer (VSM) at the IRM. Magnetic anisotropy measurements are presented in Table 1.

MAGNETIC SUSCEPTIBILITY

The magnetic susceptibility (k_{ij}) is the dimensionless proportionality factor between the magnitude of induced magnetic intensity (M_i) and the applied magnetic field strength (H_j):

$$M_i = k_{ij}H_j \text{ (Nye, 1985),}$$

where k_{ij} is a second-rank symmetric tensor that can be visualized by an ellipsoid. The principal axes of the magnetic susceptibility ellipsoid are $k_{max} \geq k_{int} \geq k_{min}$ (e.g., Hrouda, 1982). Bulk susceptibility is defined as

$$k = (k_{max} + k_{int} + k_{min})/3 \text{ (Nagata, 1961).}$$

The ratio

$$P = k_{max}/k_{min} \text{ (Nagata, 1961)}$$

is used to quantify the degree of anisotropy. SI volume units are used throughout.

The ellipsoids are represented in two types of diagrams that plot the principal values (directions and magnitudes): (1) lower hemisphere equal area stereograms of the principal directions using the conventions proposed by Ellwood et al. (1988) and (2) Flinn-type diagrams (Flinn, 1962) of the ellipsoid shape in the two-dimensional space.

SOURCES OF MAGNETIC SUSCEPTIBILITY

We applied two methods to investigate the sources of magnetic susceptibility: (1) the comparison between high-field (k_{HF}) and low-field (k_{LF}) susceptibility (Rochette and Fillion, 1988; Hrouda and Jelinek, 1990), and (2) thermomagnetic behavior (e.g., Bina and Henry, 1990; Schmidt, 1993) using k vs. temperature $k(T)$ curves. A discussion and comparison of both methods is given in Richter and van der Pluijm (1994). In high magnetic fields (1–1.5 T), above the saturation magnetization of the ferrimagnetic minerals, only diamagnetic (k_D), paramagnetic (k_P), and antiferromagnetic (k_{AF}) susceptibilities are measured: $k_{HF} = k_D + k_P + k_{AF}$. In low fields (0.1–0.5 mT) the ferrimagnetic minerals (k_F) also contribute to the magnetic susceptibility, so that $k_{LF} = k_F + k_D + k_P + k_{AF}$. It follows from these equations that

the ferrimagnetic contribution to magnetic susceptibility is calculated by

$$k_F = k_{LF} - k_{HF}.$$

Acquisition curves of the isothermal remanent magnetization (IRM) of samples from both sites show that magnetic saturation occurs well below 200 mT (Fig. 2), which is indicative of magnetite or maghemite. The differences in the saturation magnetization are due to the magnetite concentration. At both sites, pseudo-single-domain magnetite is the magnetic carrier mineral (for a detailed characterization of the magnetic mineralogy, see Kelso et al., Pariso et al., both this volume). At both sites, k_{HF} is between one and two orders of magnitude lower than k_{LF} (Fig. 3A, B) which demonstrates that k_F dominates the low-field magnetic susceptibility. Figure 3C shows $100[(k_{LF} - k_{HF})/k_{LF}]\%$ for Site 894 and Site 895 samples plotted vs. bulk susceptibility. The graph shows that the ferrimagnetic dominance increases with increasing bulk susceptibility which implies that the bulk susceptibility is a function of the magnetite concentration. The histogram of the bulk susceptibilities (Fig. 3C), in comparison with the percent ferrimagnetic contribution, demonstrates that the susceptibility of all samples is strongly magnetite-dominated.

Figure 4 shows two $k(T)$ curves (25°–700°C) for two samples from Sites 894 and 895. The arrow indicates the heating and the cooling parts of the curve. Both curves are essentially reversible, indicating little chemical change during the heating process. Sharp Curie temperatures (T_C) at 562°C (Sample 147-894G-20R-3, 124 cm) and 575°C (Sample 147-895E-1R-2, 125 cm) indicate the presence of magnetite with low Ti content and almost pure magnetite (T_C of pure magnetite = 580°C) (see Kelso et al., Pariso et al., both this volume). Below T_C, the magnetic susceptibility stays constant or increases slightly with increasing temperature. This behavior is typical for the thermomagnetic behavior of magnetite (e.g., Schmidt, 1993) without a paramagnetic contribution. A very shallow Hopkinson peak can be observed in both samples. A susceptibility decrease with increasing temperature following the Curie-Weiss law would indicate an influence of paramagnetic material to the bulk susceptibility (Schultz-Krutisch and Heller, 1985; Richter and van der Pluijm, 1994).

Both methods demonstrate that the dominant source of magnetic susceptibility and, hence, of magnetic susceptibility anisotropy is magnetite for both the Site 894 gabbros and gabbronorites and the Site 895 peridotites. Magnetic fabrics, therefore, represent the overall shape and distribution of magnetite in these rocks. Olivine, pyroxene, amphiboles, serpentine, ilmenite, pyrrhotite, and the diamagnetic plagioclase also contribute to some degree, but have only very minor influence on the magnetic susceptibility tensor.

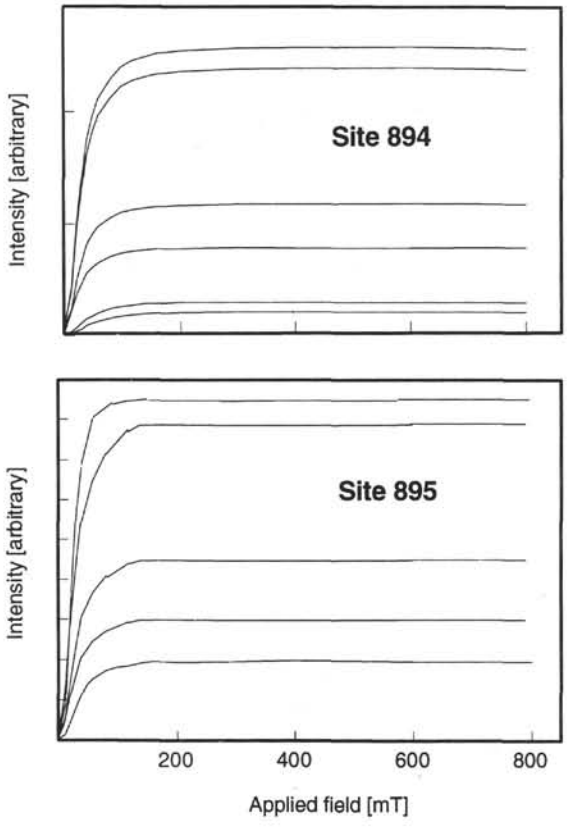

Figure 2. Acquisition curves of the isothermal remanent magnetization. Magnetic saturation for all samples occurs well below 200 mT, indicating magnetite or maghemite.

BULK SUSCEPTIBILITY

Figure 5 shows the observed magnetic bulk susceptibilities separately for the three principal holes. The values are high and range from 2.78×10^{-4} to 1.35×10^{-1}. The mean value for the Site 894 rocks is 1.72×10^{-2} and for the Site 895 peridotites, 4.29×10^{-2}, which is similar to previously reported values from oceanic mafic and ultramafic rocks (Fox and Opdyke, 1973; Kent et al., 1978). Susceptibility values between 4.27×10^{-4} and 4.32×10^{-1} have been determined from the ODP Hole 735B gabbros (Kikawa and Pariso, 1991).

The vertical distribution of magnetic susceptibilities in Holes 894G, 895D, and 895E is shown in Figure 5. Magnetite is the major source of magnetic susceptibility and, hence, variations in the magnetic susceptibility directly reflect variations in the concentration of magnetite (Kelso et al., this volume). Hole 894G shows no systematic distribution of magnetic susceptibilities with depth. A correlation between lithology (see simplified lithostratigraphic column in Fig. 5) and k does not exist. Hole 895D shows a trend towards higher susceptibilities downhole, which indicates an increase in the concentration of magnetite. Again, no relationship between k and lithology is evident. Samples from Hole 895E reach the highest observed susceptibilities and display a large scatter in bulk susceptibilities.

MAGNETIC FABRICS

Anisotropy of Magnetic Susceptibility

Ferrimagnetic minerals have a shape anisotropy that is caused by the demagnetizing field, H_{demag}, which reduces the external field H_{ext} depending on the shape and orientation of the magnetized body. The effective field H_{eff} is

$$H_{eff} = (1 / k - N)\, M$$

where N is the demagnetizing factor (e.g., Osborn, 1945). Pfleiderer and Halls (1990) investigated the relationship between shape and AMS of artificial samples and found that AMS is related inversely to the demagnetization factor, which itself relates inversely to the axial ratios of the ferrimagnetic grains. AMS provides a direct measure of the overall magnetite shape. A second mechanism to obtain a significant ferrimagnetic anisotropy is the distribution of the grains. For example, an alignment of spherical magnetite grains in a plane will lead to a higher susceptibility parallel to that plane than perpendicular to it. This phenomenon has been described as distribution anisotropy (Hargraves et al., 1991).

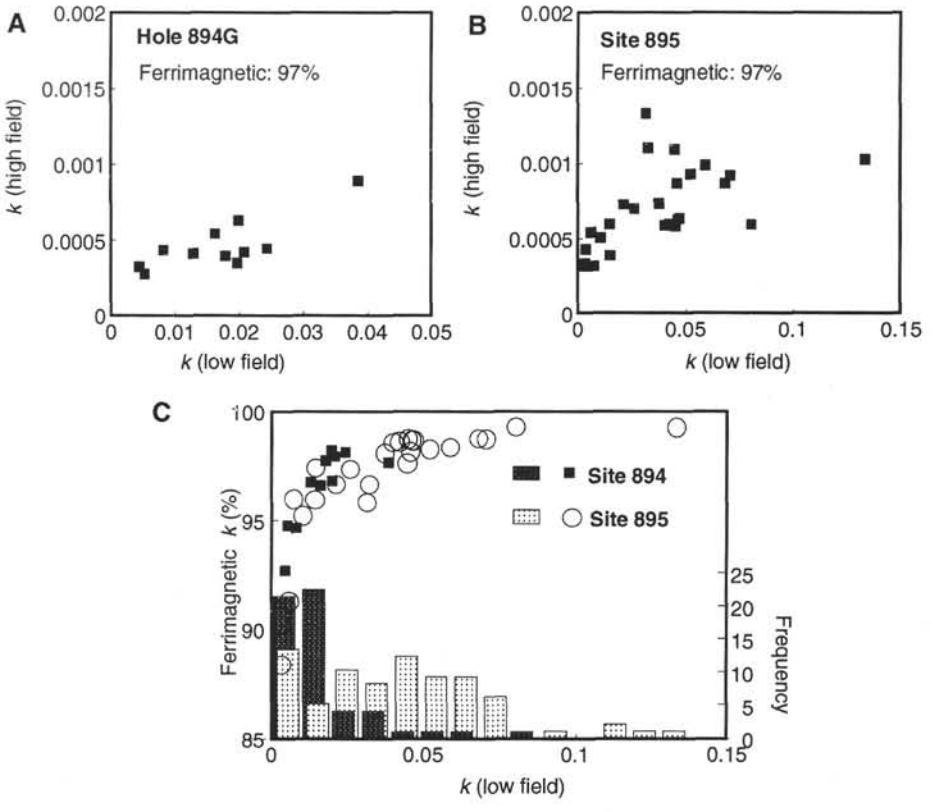

Figure 3. **A, B.** High-field susceptibility plotted vs. low-field susceptibility. The low-field susceptibility is 1–2 orders of magnitude higher, indicating a strong magnetite dominance. The contribution of ferrimagnetic magnetite to the low-field susceptibility is on average 97% at both sites. **C.** Ferrimagnetic contribution (in percent) to low-field susceptibility of individual samples plotted vs. bulk susceptibility and histogram of bulk susceptibilities. Most samples have a susceptibility that is dominated by magnetite to at least 95%.

AMS results are presented in Table 1. The magnetic anisotropy is moderate to high in most samples. Figure 6 shows the degree of anisotropy P plotted vs. depth and lithology. Anisotropies are highest in Hole 894G gabbros and there is a tendency of increasing anisotropy downhole to about 100 mbsf, where the highest anisotropies are reached. P varies between 1.01 and 1.42 (average = 1.15) at Hole 894G, between 1.03 and 1.18 (average = 1.10) at Hole 895D, and between 1.03 and 1.25 (average = 1.12) at Hole 895E. The lithology has no apparent influence on the anisotropy or on the ellipsoid shape. AMS ellipsoid shapes are presented in Flinn diagrams (Flinn, 1962) in Figure 7. The shapes of the susceptibility ellipsoids scatter between oblate, prolate, and almost isotropic. Most are triaxial, that is, they cluster around the dashed line of the Flinn diagrams ($k_{max}/k_{int} = k_{int}/k_{min}$), except that samples from Hole 895E tend toward more oblate-shaped AMS ellipsoid forms.

The rotary-drilled cores have only a vertical (no horizontal) orientation and the principal susceptibility directions appear to be random for that reason (Table 1). In addition, the complicated tectonic situation within the rift (e.g., Karson et al., 1992) adds another factor that apparently randomizes the orientation of the susceptibility ellipsoids. Stable paleomagnetic directions have an average inclination of 38° at Site 894 (Pariso et al., this volume) and no consistent inclination at Site 895 (Kelso et al., this volume), although the calculated dipole field inclination at the latitude of Hess Deep is +4.6°. This implies that major block rotations occurred, and not only the horizontal orientation but also the vertical orientation before tectonic rotation and drilling is uncertain. The dip of the principal susceptibility axes, however, should be unaffected by the lack of azimuthal control and should yield an estimate of the mean inclination of the susceptibility axes after the rift-related tectonic rotation. Figure 8 shows histograms of the dip of k_{min} for the three principal holes. At Hole 894G it is apparent that the pattern is not random and that most k_{min} axes have a shallow dip with an average of 25°. The k_{min} distribution at Hole 895D is very scattered and shows no significant maximum. The scatter is also considerable at Hole 895E but a distinct maximum is reached at 30°. The dip of k_{min} is generally shallow and shows a very systematic distribution at Holes 894G and 895E. This suggests that the orientation of the AMS ellipsoids in a geographical reference frame bear a geological significance.

Anisotropy of Anhysteretic Remanent Magnetization

ARM anisotropy measures a remanent magnetization and, hence, determines the fabric of the carriers of remanence, that is, magnetite only (Kelso et al., Pariso et al., both this volume). We have demonstrated that AMS is also dominated by magnetite. Both methods should yield a comparable result if the measured effective magnetic grain size is the same. Figure 9 compares the AMS and the AARM ellipsoids of three samples from the three main holes. Figure 9A shows the magnetic fabrics of a gabbronorite from Hole 894G. The shape of the prolate ellipsoids and the orientations of the principal directions are virtually the same, but P_{AMS} is higher than P_{AARM}. A harzburgite sample from Hole 895D (Fig. 9B) has triaxial ellipsoid shapes and the principal directions of the AMS and AARM ellipsoids are only a few degrees apart. The dunite sample from Hole 895E (Fig. 9C) has a strongly oblate fabric. P_{AARM} is 1.38 and very strong compared to $P_{AMS} = 1.02$, which is typical of the methods (Jackson, 1991). The orientation of the minimum axes is virtually identical, whereas

the maximum and intermediate directions are rotated, as can be expected for a strongly oblate ellipsoid, on a great circle perpendicular to k_{min}. Reasons for the deviation between the two tensors are that (1) AMS, though it is dominated by magnetite, is also influenced by paramagnetic and diamagnetic susceptibilities, and (2) AARM and AMS do not measure the same effective magnetic grain size.

DISCUSSION

The orientation of the magnetic fabric of ultramafic rocks has been demonstrated to be related to structural features and flow patterns (Smith and Banerjee, 1985; MacDonald and Ellwood, 1988; Bina et al., 1990; Wagner et al., 1981). The macroscopic fabrics of the gabbroic rocks collected at Site 894 are either isotropic or foliated. The foliation is defined by the shape-preferred orientation of crystals, mainly plagioclase, and is related to magmatic flow (Gillis, Mével, Allan, et al., 1993). In contrast to samples from Hole 735B (ODP Leg 118), the rocks show little evidence for solid-state penetrative deformation. The orientation of the near-vertical foliation is generally north–south with a steeply plunging lineation (Fig. 10; MacLeod, Boudier, et al., this volume).

Figure 11 shows the principal susceptibility axes of foliated gabbros from Hole 894G. The data are corrected for the stable magnetic remanence (Kelso et al., this volume; Pariso et al., this volume), that is, to a common declination (0°, normal polarity) and inclination (+4.6°, the calculated dipole field inclination for the latitude of Hess Deep). A comparison with the structural data from Figure 10 shows that k_{max} is parallel to the mineral lineation and that k_{min} is parallel to the poles of foliation. k_{max} has a steeply dipping orientation and scatters on a great circle within the foliation plane. k_{int} and k_{min} are shallow-dipping. The magnetic fabric is directly related to the rock fabric, though the rock fabric is defined by the shape-preferred orientation of mainly plagioclase, which does not significantly contribute to AMS.

We have used this relationship to investigate the fabrics of macroscopically isotropic-looking gabbro samples from Hole 894G (Fig. 12). Compared to the fabric diagrams (Fig. 10) and the magnetic fab-

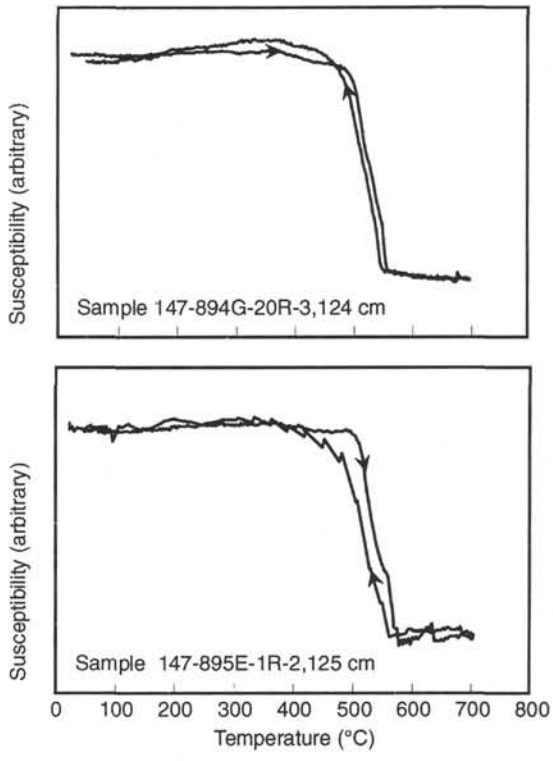

Figure 4. Heating and cooling curves of low-field susceptibility. Arrows indicate heating and cooling part of curve. No temperature dependence of the susceptibility before the intensity breakdown at the Curie temperature indicates that only ferrimagnetic magnetite contributes significantly to magnetic susceptibility. Both curves are virtually reversible, indicating little chemical change during heating. The Hopkinson peak is very shallow in both samples.

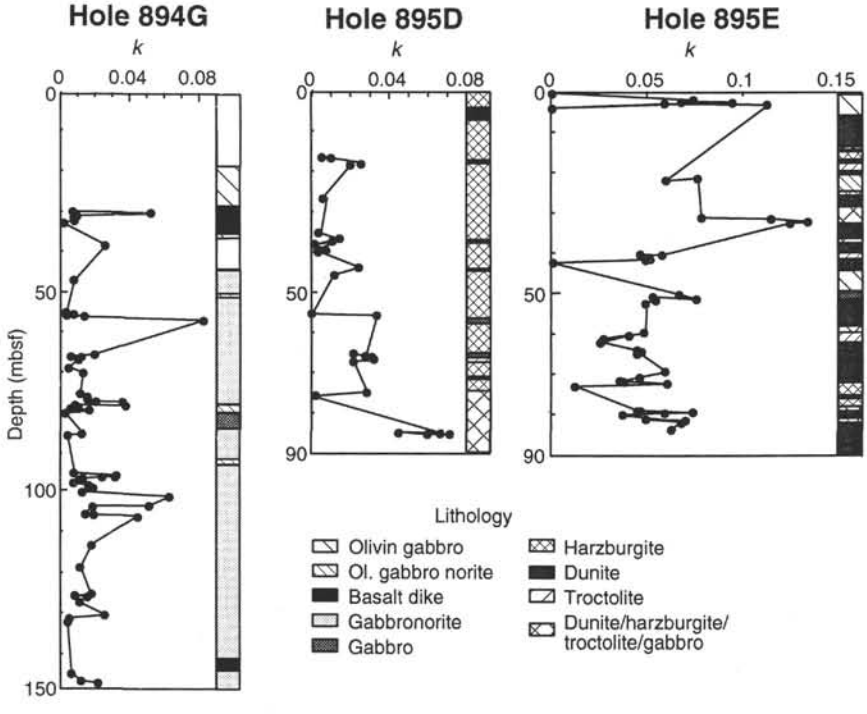

Figure 5. Bulk susceptibility plotted vs. depth and simplified lithology. The susceptibility magnitude is directly related to magnetite concentration.

Table 1. Anisotropy of magnetic susceptibility.

Core, section, interval (cm)	Depth (mbsf)	k_{min}	D	I	k_{int}	D	I	k_{max}	D	I
147-894G-										
1R-1, 17	18.77	0.009682	354	7	0.009872	103	71	0.010001	262	18
2R-1, 68	29.28	0.007191	266	13	0.007242	111	76	0.007273	357	6
2R-2, 57	31.00	0.008154	205	17	0.008201	110	17	0.008294	337	66
2R-2, 110	31.20	0.008576	155	36	0.008617	27	40	0.008643	269	26
2R-3, 32	31.87	0.001909	240	39	0.001925	351	24	0.001962	105	41
2R-3, 118	32.73	0.025727	276	12	0.026494	174	44	0.027159	18	43
3R-1, 6	38.26	0.007765	114	9	0.008110	42	53	0.008155	241	35
4R-2, 76	47.10	0.003680	343	1	0.003749	253	2	0.003910	96	88
6R-1, 26	55.06	0.007117	181	13	0.007258	280	36	0.007675	75	51
6R-1, 77	55.57	0.003983	87	25	0.004012	196	35	0.004234	329	44
6R-1, 89	55.69	0.013002	125	60	0.013465	347	23	0.015203	249	18
6R-2, 0	56.23	0.073723	11	38	0.082886	129	31	0.092105	245	37
6R-2, 78	57.01	0.018297	135	5	0.019456	36	58	0.020897	228	31
7R-1, 99	65.79	0.005977	68	6	0.006515	162	30	0.006848	328	60
7R-2, 6	66.26	0.010913	4	1	0.012157	94	18	0.013320	269	71
7R-2, 10	66.30	0.010426	109	18	0.010964	214	37	0.011352	359	47
7R-2, 61	66.81	0.004672	136	15	0.004948	302	74	0.005118	45	4
8R-1, 54	69.04	0.012894	280	22	0.013255	73	66	0.013721	186	10
8R-2, 31	70.31	0.010738	195	20	0.011809	97	21	0.012133	325	61
9R-1, 120	75.60	0.014910	257	15	0.015741	9	54	0.016542	158	32
9R-2, 86	76.51	0.014733	16	82	0.016248	206	8	0.016689	116	1
9R-3, 19	77.10	0.018961	140	21	0.020385	50	2	0.022016	314	69
9R-3, 69	77.60	0.033191	301	32	0.035920	208	4	0.039759	112	57
9R-3, 77	77.68	0.034741	258	22	0.036526	350	6	0.043481	95	67
9R-4, 45	78.78	0.007985	330	37	0.008626	126	51	0.009018	231	12
9R-4, 90	78.42	0.004899	228	34	0.005326	328	15	0.005803	78	52
9R-4, 95	79.28	0.010543	217	35	0.011093	95	37	0.011338	335	34
9R-4, 130	79.63	0.016311	338	54	0.016999	242	4	0.017630	149	35
10R-1, 81	79.91	0.016455	56	25	0.016786	325	2	0.017249	230	65
10R-1, 91	80.01	0.003037	50	29	0.003088	267	56	0.003141	150	17
10R-2, 8	80.56	0.012109	174	57	0.013503	16	31	0.014133	280	10
11R-2, 34	85.90	0.004248	289	45	0.004442	165	29	0.004861	56	31
11R-2, 45	86.01	0.007541	20	12	0.008417	283	31	0.009172	129	56
12R-2, 50	95.76	0.026285	70	14	0.035195	297	70	0.036316	164	14
12R-2, 111	96.37	0.030509	47	35	0.032332	139	3	0.033250	234	54
12R-2, 140	96.66	0.022597	300	40	0.024185	174	35	0.027179	59	31
12R-3, 4	96.77	0.011477	30	15	0.012552	291	30	0.013630	143	56
12R-3, 48	97.21	0.009886	266	20	0.011008	360	9	0.011955	113	67
12R-3, 67	97.40	0.007804	252	32	0.007948	346	6	0.008955	85	57
12R-4, 20	98.43	0.014889	0	4	0.016259	269	16	0.019096	103	73
12R-4, 51	98.74	0.018586	142	28	0.018874	242	18	0.020980	360	56
12R-4, 139	99.62	0.012038	348	2	0.012685	80	7	0.013907	188	69
12R-5, 79	100.52	0.056704	225	24	0.063521	328	28	0.071084	101	52
12R-6, 39	101.56	0.042575	123	46	0.053227	263	36	0.058540	10	21
13R-1, 59	103.99	0.015257	112	34	0.019607	319	52	0.021625	211	13
13R-1, 62	104.02	0.014049	290	60	0.014790	31	6	0.015442	125	29
13R-2, 120	105.97	0.018611	171	10	0.019705	264	14	0.020690	46	73
13R-3, 5	106.28	0.040547	31	14	0.045019	136	45	0.050484	288	41
13R-3, 30	106.53	0.015530	288	6	0.018679	23	35	0.021166	190	54
14R-1, 70	113.80	0.011136	58	37	0.012130	160	15	0.012514	268	49
15R-1, 73	119.53	0.017141	158	24	0.018298	302	61	0.018384	61	15
17R-1, 60	126.40	0.008181	342	15	0.008534	84	38	0.008982	235	48
17R-1, 90	126.70	0.013377	116	21	0.015380	334	64	0.017471	212	14
17R-1, 123	127.03	0.010749	10	54	0.011128	269	7	0.011419	174	35
17R-2, 114	128.38	0.024927	61	23	0.025940	307	42	0.027803	171	38
18R-1, 69	131.59	0.004416	83	14	0.004978	349	16	0.005231	212	69
18R-2, 7	132.39	0.004308	75	26	0.004508	178	23	0.004733	303	53
18R-2, 94	133.26	0.006444	104	7	0.006481	348	74	0.006833	195	15
20R-1, 69	146.20	0.011930	181	19	0.012230	52	62	0.012860	278	20
20R-3, 56	147.98	0.020764	16	79	0.021536	261	5	0.022212	170	10
20R-3, 124	148.66	0.006438	270	21	0.006599	42	61	0.006729	172	20
147-895D-										
2R-1, 25	16.20	0.005899	104	5	0.006239	215	76	0.006498	13	13
2R-1, 47	16.47	0.010184	230	8	0.010338	230	8	0.010517	334	62
2R-2, 39	17.81	0.023973	97	23	0.026505	347	38	0.027687	211	43
2R-2, 51	17.93	0.033789	103	17	0.037173	348	54	0.038664	203	31
2R-2, 78	18.20	0.019802	103	5	0.020139	197	32	0.021140	5	57
3R-1, 45	26.45	0.005415	222	31	0.005987	129	6	0.006055	29	58
4R-1, 41	35.11	0.003690	171	33	0.003796	27	51	0.003923	273	18
4R-3, 4	37.03	0.010206	156	5	0.010793	256	62	0.011579	64	28
4R-3, 10	38.09	0.002410	233	9	0.002478	339	59	0.002528	137	29
4R-3, 15	37.14	0.013798	285	20	0.014142	32	39	0.015187	174	44
4R-4, 84	39.29	0.003375	297	35	0.003487	60	37	0.003704	180	33
4R-4, 100	39.45	0.007705	182	4	0.008005	89	43	0.008210	277	47
4R-5, 3	39.76	0.004655	53	72	0.004868	178	11	0.005009	271	15
4R-5, 8	39.81	0.003430	46	74	0.003574	207	15	0.003627	298	5
5R-1, 52	43.82	0.023074	294	65	0.024921	158	19	0.026079	62	16
5R-2, 100	45.74	0.010961	219	46	0.011570	312	2	0.011831	44	44
6R-1, 32	55.32	0.000343	317	21	0.000347	58	25	0.000354	192	56
6R-1, 75	55.75	0.031261	306	40	0.034179	57	23	0.035167	169	41
7R-1, 65	65.25	0.020026	300	34	0.020980	84	50	0.022334	197	19
7R-1, 119	65.79	0.026965	293	26	0.027945	83	61	0.028858	197	13
7R-2, 13	66.20	0.030171	151	24	0.031281	304	64	0.032577	56	11
7R-2, 92	66.99	0.029363	350	82	0.033403	187	8	0.034673	97	2
7R-2, 107	67.14	0.019491	352	88	0.022111	130	2	0.022828	220	1
8R-1, 45	74.75	0.027632	75	17	0.028665	339	20	0.029296	203	63
8R-2, 4	75.72	0.000304	342	10	0.000316	84	49	0.000319	243	39

Table 1 (continued).

Core, section, interval (cm)	Depth (mbsf)	k_{min}	D	I	k_{int}	D	I	k_{max}	D	I
9R-1, 12	85.20	0.062438	71	23	0.068765	327	30	0.070493	192	51
9R-1, 78	84.78	0.043314	313	50	0.043829	76	25	0.047916	182	29
9R-1, 129	85.29	0.055846	300	18	0.061605	59	56	0.062942	200	28
9R-1, 140	85.40	0.068155	174	6	0.070881	58	77	0.074283	265	11
147-895E-										
1R-1, 47	0.47	0.000315	66	48	0.000323	167	10	0.000325	265	41
1R-2, 72	2.16	0.072891	60	23	0.074641	321	22	0.075923	192	57
1R-2, 105	2.49	0.063194	107	50	0.070492	223	21	0.071859	327	33
1R-2, 125	2.69	0.090723	85	43	0.094869	247	46	0.099498	347	9
1R-3, 24	3.10	0.055829	51	60	0.059819	247	29	0.064188	153	7
1R-3, 49	3.35	0.102041	289	73	0.117697	94	16	0.120624	185	4
1R-3, 122	4.08	0.000430	284	48	0.000446	191	3	0.000454	98	42
2R-2, 56	21.52	0.074210	20	50	0.075420	154	30	0.081020	259	24
2R-2, 107	22.03	0.055142	271	33	0.059278	61	53	0.065181	171	15
3R-2, 24	31.21	0.072360	269	15	0.080761	139	67	0.083009	4	17
3R-2, 55	31.52	0.102066	244	30	0.121179	58	60	0.123003	152	3
3R-2, 136	32.33	0.122954	324	53	0.139550	98	28	0.143662	200	23
3R-3, 14	32.61	0.113759	318	68	0.127766	183	16	0.134663	89	15
4R-1, 92	40.42	0.041734	60	16	0.045126	289	67	0.051814	155	17
4R-1, 102	40.52	0.056330	56	27	0.058639	265	60	0.060351	153	12
4R-2, 46	41.40	0.047680	170	17	0.051147	60	48	0.051368	273	37
4R-2, 58	41.52	0.049431	331	24	0.052156	218	41	0.054088	82	39
4R-3, 6	42.47	0.000275	46	23	0.000277	142	13	0.000283	260	63
5R-1, 145	50.35	0.064530	19	2	0.066682	111	34	0.071141	286	56
5R-2, 48	50.88	0.051276	233	36	0.053713	360	40	0.055516	118	30
5R-2, 115	51.55	0.068638	38	70	0.079283	196	19	0.081000	289	7
5R-2, 132	51.72	0.050901	49	10	0.056716	178	74	0.057332	317	13
5R-3, 35	52.25	0.046235	244	22	0.051501	111	60	0.052380	342	20
6R-1, 131	59.91	0.047098	186	23	0.049742	73	43	0.050929	295	38
6R-2, 21	60.31	0.038364	252	35	0.041357	45	52	0.043945	152	13
6R-2, 111	61.21	0.026074	110	33	0.027689	290	57	0.027906	20	0
6R-3, 68	61.99	0.023587	253	40	0.025416	32	42	0.025903	142	22
6R-3, 101	62.32	0.023927	298	25	0.025829	88	62	0.026654	202	12
6R-5, 40	64.15	0.042473	163	26	0.046932	256	6	0.047908	359	64
6R-5, 66	64.41	0.044620	333	10	0.046553	82	63	0.048249	238	25
6R-5, 74	64.49	0.044080	320	10	0.048291	51	5	0.049166	168	79
6R-5, 95	64.70	0.044158	300	4	0.045345	34	37	0.047818	205	53
7R-1, 135	69.55	0.055826	180	7	0.061959	313	81	0.062697	90	7
7R-2, 10	70.72	0.043251	100	71	0.046670	7	1	0.049420	277	19
7R-3, 39	71.59	0.035240	166	56	0.038112	259	2	0.040418	350	34
7R-3, 60	71.80	0.033780	339	45	0.035472	109	33	0.037668	218	27
7R-3, 125	72.45	0.057050	15	49	0.062849	254	24	0.064526	148	31
7R-4, 36	73.06	0.012020	145	40	0.012748	6	42	0.013452	254	22
8R-1, 113	79.03	0.042607	84	39	0.045819	338	19	0.047486	228	45
8R-1, 120	79.10	0.044156	83	28	0.047930	253	62	0.051263	351	4
8R-2, 16	79.55	0.067631	130	35	0.074519	247	33	0.079302	7	37
8R-2, 57	79.69	0.058025	55	30	0.058913	172	39	0.060683	299	37
8R-2, 70	80.09	0.036113	198	24	0.038267	339	60	0.039092	100	17
8R-2, 90	80.29	0.035280	59	31	0.037336	157	13	0.039186	266	55
8R-3, 51	81.31	0.047464	104	45	0.049822	257	42	0.050911	360	14
8R-3, 66	81.46	0.060482	185	28	0.073245	281	10	0.075780	29	60
8R-3, 103	81.83	0.065203	114	51	0.069471	345	27	0.070559	240	26
8R-4, 118	83.48	0.061090	229	18	0.063773	3	65	0.064851	133	17

Notes: AMS measurements in SI units (volume susceptiblity). D = declination in degrees; I = inclination in degrees (core coordinates).

rics of the foliated gabbros (Fig. 11), the magnetic fabrics of the unfoliated samples show the same characteristics. k_{max} dips steeply to the northeast. The distribution of k_{min} and k_{int} is more scattered. Most k_{min} axes have an east to northeast direction and most k_{int} axes dip shallowly to the south. Though a macroscopic fabric is not visible, we can infer from the magnetic fabric data that the isotropic gabbros have a steeply dipping magmatic lineation and north–south-oriented foliation. These structures are too weakly developed to be visible but can be detected with sensitive petrofabric indicators, like AMS.

We argue, that the process for the development of the AMS is a distribution anisotropy (Wolff et al., 1989; Hargraves et al., 1991; Stephenson, 1994). Magnetic grains do not have to be nonequant (elliptical, elongated, or flattened) and aligned in order to impart a detectable AMS. The effect may arise through organization of equant, irregular, or skeletal grains into planar or linear arrangements. It is not necessary that the grains actually grow during the magma flow period (and thus acquire a shape anisotropy), it is enough that the grains are arranged or grow along preexisiting fabric elements. Hargraves et al. (1991) argue that AMS in pristine igneous rocks is a direct or indirect reflection of preexisting silicate fabric, which is associated with flow or intrusion of the magma. They conclude that AMS provides a direct record of fluid-dynamic histories of igneous rocks. The Hole 894G plutonic rocks contain primary igneous magnetite and ilmenite, which are now affected by exsolution and alteration. Thin sections show that the texture of the oxide minerals is predominantly interstitial, and equant in coarser and less deformed patches (Gillis, Mével, Allan, et al., 1993). The late-crystallizing interstitial minerals form thin cuspate-shaped grains between the silicates, partially or totally enclose silicates, or, where interstitial between plagioclase, make up subangular cross sections. The distribution of these grains will be relatively anisotropic if they grew in residual liquid volumes within a preferredly oriented (by magmatic flow) silicate (i.e., a plagioclase "template"). This mechanism explains (1) the origin of magnetic anisotropy in mafic and ultra mafic rocks from Hess Deep and (2) why macroscopic plagioclase fabrics and magnetite fabrics caused by interstitial and sometimes equant grains are parallel.

Magnetic fabric data demonstrate that the gabbros (Figs. 11 and 12) have a very uniform fabric with a steeply dipping magnetic/magmatic lineation and a near-vertical foliation (the plane perpendicular to k_{min}). The average strike of the foliation is approximately north–south, that is, parallel to the strike of the EPR spreading axis. Sheeted

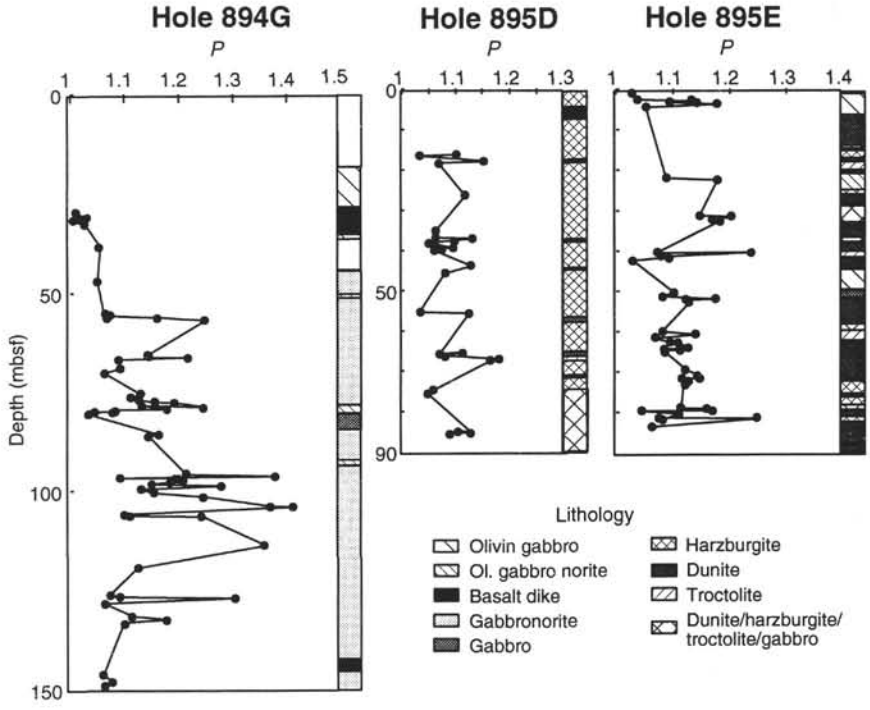

Figure 6. The degree of anisotropy $P = k_{max}/k_{min}$ plotted vs. depth and simplified lithology.

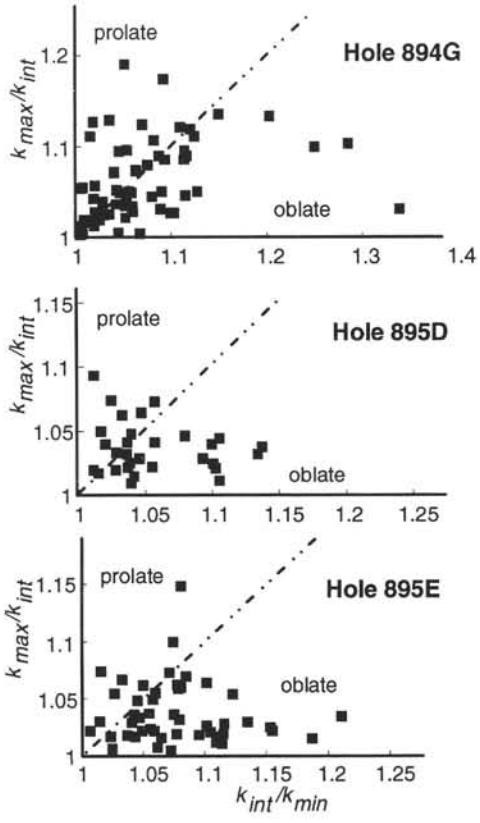

Figure 7. The shape of the magnetic susceptibility ellipsoid in Flinn diagrams. Most ellipsoids are triaxial; samples from Hole 895E have more oblate-shaped susceptibility ellipsoids.

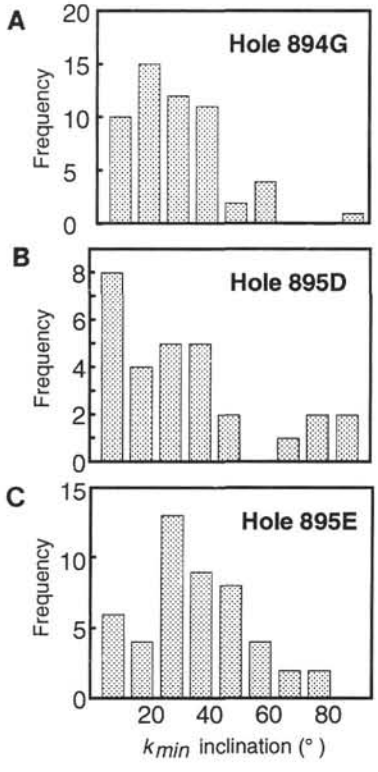

Figure 8. Histograms of the inclination of the minimum susceptibility axes of the three principal holes. **A.** The dip of k_{min} of the Hole 894G rocks is shallow, about 25° on average. **B.** Hole 895D shows a large k_{min} scatter and no apparent maximum. **C.** Hole 895E samples show a large scatter, but have a distinct maximum at 30°.

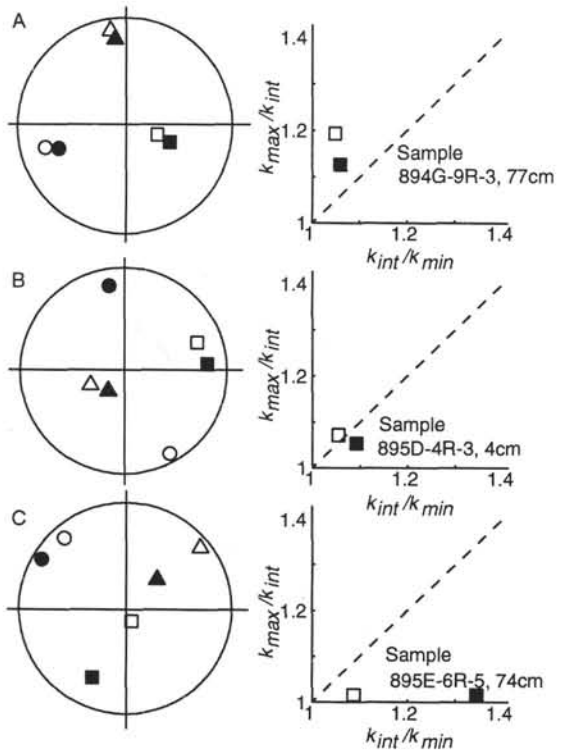

Figure 9. Comparison between AMS and AARM ellipsoids for selected samples. Square = maximum; triangle = intermediate; circle = minimum direction; open symbols = AMS; solid symbols = AARM. **A, B.** The principal directions and shapes of both ellipsoids compare well. **C.** The differences in orientation and degree of anisotropy demonstrate that for this sample both methods measure a different effective magnetic grain size.

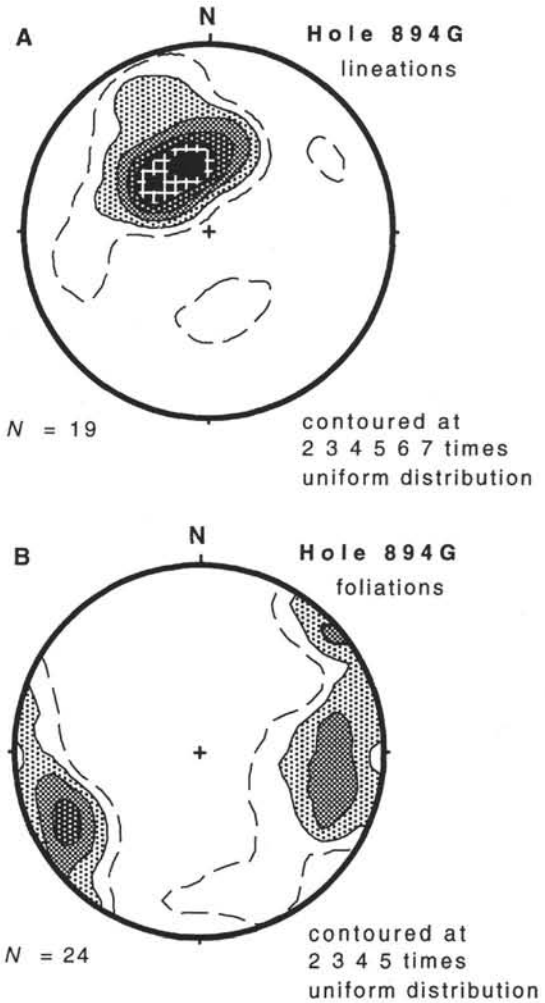

Figure 10. Structural features of foliated gabbros from Hole 894G (from MacLeod, Boudier, et al., this volume). **A.** Steeply dipping lineations. **B.** Magmatic foliations that are near-vertical and strike north–south, approximately parallel to the EPR axis.

dikes measured on the north wall of Hess Deep during *Alvin* dives (Karson et al., 1992) are near-vertical and also have an EPR-parallel north–south orientation. The steep lineations and foliations in the gabbros parallel to those in the sheeted dike complex have been interpreted to record the upward flow of melt at the top of the axial magma chamber into the base of a sheeted dike complex (Nicolas et al., 1988; MacLeod and Rothery, 1992).

Peridotites from Site 895 yielded no consistent stable paleomagnetic direction (Kelso et al., this volume). The dip of k_{min} in the unrotated data is very scattered, and a relationship between macroscopic features and AMS is not apparent. The randomly distributed secondary magnetite that was formed during the serpentinization process presumably randomizes the magnetic fabric and overprints any meaningful relationships between tectonic structures and magnetic fabrics.

CONCLUSIONS

Our magnetic fabric study of mafic and ultramafic rocks from Hess Deep demonstrates that AMS is a very sensitive method that can be used to identify and characterize rock fabrics even in rocks that appear to be macroscopically isotropic. In detail we demonstrated that:

1. High-field/low-field comparisons and thermomagnetic behavior show that magnetic susceptibilities (and, hence, magnetic fabrics) are dominated by magnetite.

2. Magnetic susceptibility anisotropy presumably originates from a distribution anisotropy which is caused by the growth of magnetite grains into a preexisiting silicate flow fabric. The degree of anisotropy is moderate to high (average k_{max}/k_{min} = 1.15 at Hole 894G, 1.10 at Hole 895D, and 1.12 at Hole 895E), susceptibility ellipsoids are in general triaxial. Lithology has no apparent influence on the shape of the anisotropy ellipsoid.

3. Anisotropies of remanence (AARM) and of susceptibility (AMS) both measure the overall preferred orientation or shape anisotropy of magnetite grains. The effective grain size determined by both methods is different, however, and orientation and shape of the anisotropy ellipsoids differ for that reason.

4. The mean dip of the minimum susceptibility axes after tectonic rotation due to rifting is 25° for the Hole 894 gabbroic rocks.

5. We did not observe a relationship between structural features and magnetic fabrics for the Site 895 peridotites. The formation of randomly oriented secondary magnetite during the serpentinization process obliterates any meaningful correlation between structural features and magnetic fabrics.

6. Rotation of the AMS directions of foliated gabbros from Site 894 into a common stable paleomagnetic direction (declination and inclination) shows that k_{min} is perpendicular to the observed magmatic foliation and k_{max} parallel to the magmatic lineation. The lineation is dipping steeply to the northeast and the foliation has a north–south

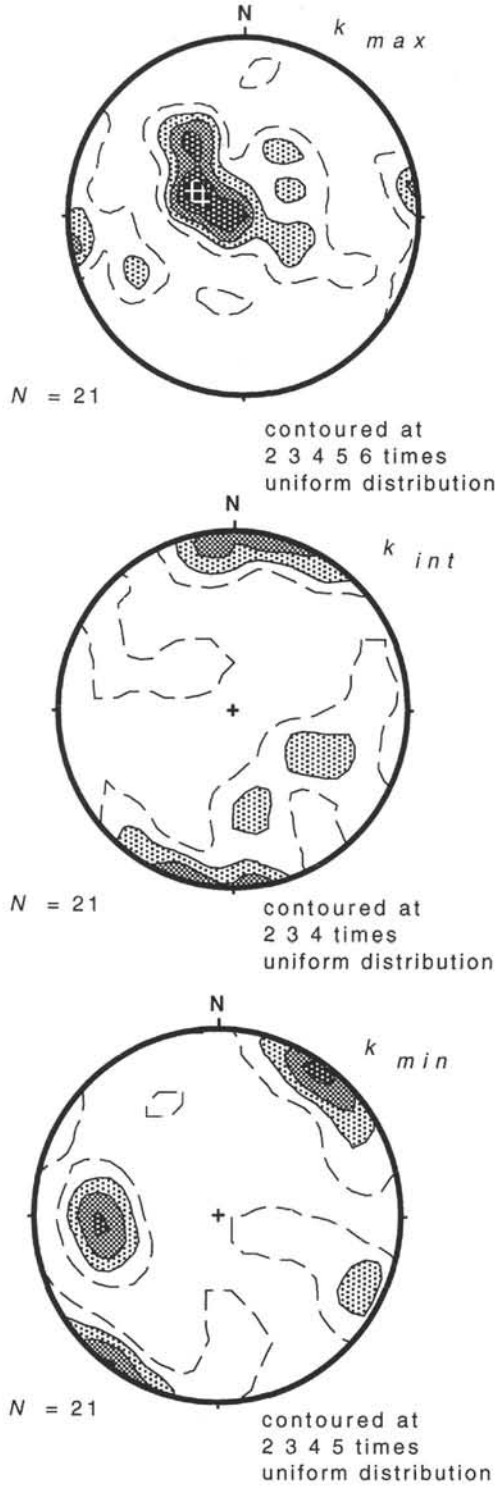

Figure 11. Principal magnetic susceptibility axes of macroscopically foliated gabbroic rocks from Hole 894G. Values are restored to a common stable magnetic declination and inclination. k_{max} has a steep inclination that is parallel to the magmatic lineation and k_{min} a shallow inclination that is parallel to the poles to planes of the foliated gabbros (compare to Fig. 10).

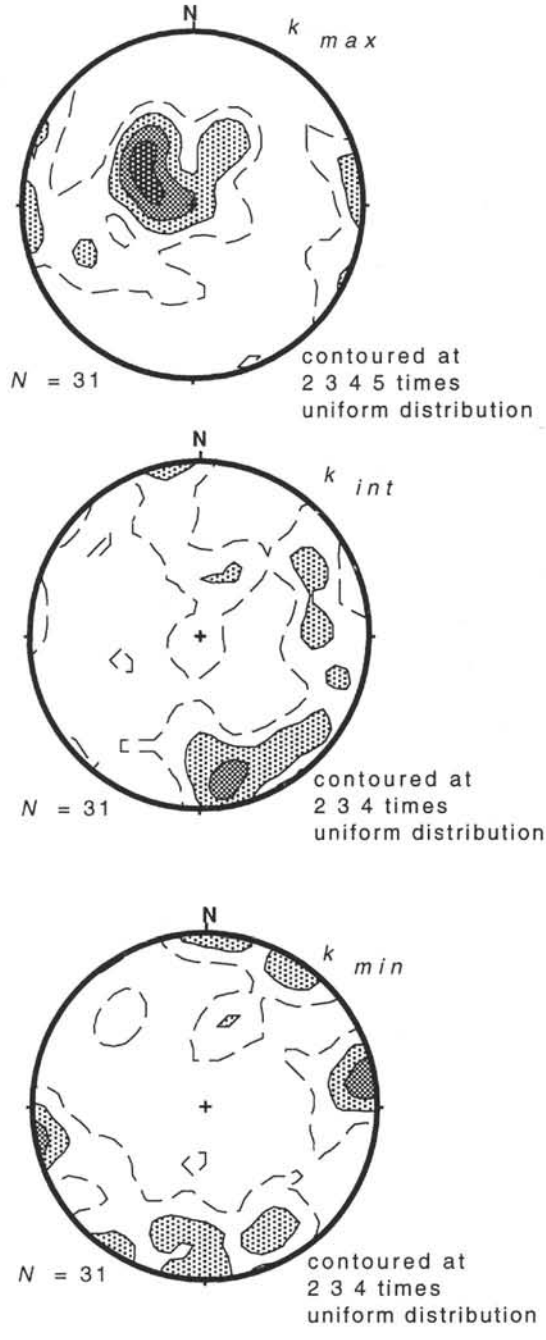

Figure 12. Principal magnetic susceptibility axes of macroscopically isotropic gabbroic rocks from Hole 894G. Values are restored to a common stable magnetic declination and inclination. The orientation of the axes is the same as in the macroscopically foliated rocks and parallel to the lineation and foliation observed in the foliated gabbros.

strike that is parallel to the EPR. Rock fabrics are defined by the preferred orientation of plagioclase and magnetic fabrics determine the preferred orientation/distribution of magnetite.

7. Macroscopically isotropic gabbros have the same magnetic fabrics as the foliated gabbros. The minimum susceptibility axes are oriented about east–west and the maximum axes are near-vertical.

8. Structural and magnetic fabric data reveal a preferred orientation with an EPR parallel strike and a steep inclination. The rocks

show little evidence for penetrative deformation and the structures are interpreted to represent magmatic flow fabrics. These fabrics are parallel to structures determined in the sheeted dikes from the north wall of Hess Deep (Karson et al., 1992) and can be interpreted to record the upward flow of melt at the top of the axial magma chamber into the base of a sheeted dike complex.

ACKNOWLEDGMENTS

Rock magnetic measurements were carried out at the Institute for Rock Magnetism (University of Minnesota). The IRM is funded by the Keck Foundation, the National Science Foundation, and the University of Minnesota. We thank Chris Hunt and Jim Marvin for their support. The thermomagnetic curves could not have been included without the help of Peat Solheid. We thank Peter Clift and reviewers Brooks Ellwood, Bernie Housen, Jamie Allan, and Shanna Collie for helpful comments on our manuscript. Shipboard scientists F. Boudier, B. Célérier, L. Kennedy, E. Kikawa, and J. Pariso contributed structural and paleomagnetic data. Research was supported by the Deutsche Forschungsgemeinschaft, grant RI576/1-2 (C.R.), USSSP grant 147-20719b (P.K.), and the Natural Environment Research Council (C.J.M.).

REFERENCES

Bina, M.M., and Henry, B., 1990. Magnetic properties, opaque mineralogy and magnetic anisotropies of serpentinized peridotites from ODP Hole 670A near the Mid-Atlantic Ridge. *Phys. Earth Planet. Inter.,* 65:88–103.

Bina, M.M., Henry, B., and Cannat, M., 1990. Magnetic anisotropy and some other magnetic properties of serpentinized peridotites from ODP Hole 670A. *In* Detrick, R., Honnorez, J., Bryan, W.B., Juteau, T., et al. *Proc. ODP, Sci. Results,* 106/109: College Station, TX (Ocean Drilling Program), 263–267.

Borradaile, G.J., 1988. Magnetic susceptibility, petrofabrics and strain. *Tectonophysics,* 156:1–20.

Borradaile, G.J., and Werner, T., 1994. Magnetic anisotropy of some phyllosilicates. *Tectonophysics,* 235:223–248.

Ellwood, B.B., Hrouda, F., and Wagner, J.-J., 1988. Symposia on magnetic fabrics: introductory comments. *Phys. Earth Planet. Inter.,* 51:249–252.

Ernst, R.E., and Baragar, W.R.A., 1992. Evidence from magnetic fabric for the flow pattern of magma in the Mackenzie giant radiating dike swarm. *Nature,* 356:511–513.

Flinn, D., 1962. On folding during three-dimensional progressive deformation. *Q. J. Geol. Soc. London,* 118:385–433.

Fox, P.J., and Opdyke, N.D., 1973. Geology of the oceanic crust: magnetic properties of oceanic rocks. *J. Geophys. Res.,* 78:5139–5154.

Francheteau, J., Armijo, R., Cheminée, J.L., Hekinian, R., Lonsdale, P., and Blum, N., 1990. 1 Ma East Pacific Rise oceanic crust and uppermost mantle exposed by rifting in Hess Deep (equatorial Pacific Ocean). *Earth Planet. Sci. Lett.,* 101:281–295.

Gillis, K., Mével, C., Allan, J., et al., 1993. *Proc. ODP, Init. Repts.,* 147: College Station, TX (Ocean Drilling Program).

Girdler, R.W., 1961. The measurement and computation of anisotropy of magnetic susceptibility of rocks. *Geophys. J. R. Astron. Soc.,* 5:34–44.

Hargraves, R.B., Johnson, D., and Chan, C.Y., 1991. Distribution anisotropy: the cause of AMS in igneous rocks? *Geophys. Res. Lett.,* 18:2193–2196.

Housen, B.A., and van der Pluijm, B.A., 1990. Chlorite control of correlations between strain and anisotropy of magnetic susceptibility. *Phys. Earth Planet. Inter.,* 61:315–323.

Hrouda, F., 1982. Magnetic anisotropy of rocks and its application in geology and geophysics. *Geophys. Surv.,* 5:37–82.

Hrouda, F., and Jelinek, V., 1990. Resolution of ferrimagnetic and paramagnetic anisotropies in rocks, using combined low-field and high-field measurements. *Geophys. J. Int.,* 103:75–84.

Hrouda, F., and Schulman, K., 1990. Conversion of the magnetic susceptibility tensor into the orientation tensor in some rocks. *Phys. Earth Planet. Inter.,* 63:71–77.

Jackson, M., 1991. Anisotropy of magnetic remanence: a brief review of mineralogical sources, physical origins, and geological applications, and comparison with susceptibility anisotropy. *Pure Appl. Geophys.,* 136:1–28.

Karson, J.A., Hurst, S.D., and Lonsdale, P.F., 1992. Tectonic rotations of dikes in fast-spread oceanic crust exposed near Hess Deep. *Geology,* 20:685–688.

Kent, D.V., Honnorez, B.M., Opdyke, N.D., and Fox, P.J., 1978. Magnetic properties of dredged oceanic gabbros and source of marine magnetic anomalies. *Geophys. J. R. Astron. Soc.,* 55:513–537.

Kikawa, E., and Pariso, J.E., 1991. Magnetic properties of gabbros from Hole 735B, Southwest Indian Ridge. *In* Von Herzen, R.P., Robinson, P.T., et al., *Proc. ODP, Sci. Results,* 118: College Station, TX (Ocean Drilling Program), 285–307.

Lonsdale, P., 1988. Structural pattern of the Galapagos microplate and evolution of the Galapagos triple junction. *J. Geophys. Res.,* 93:13551–13574.

MacDonald, W.D., and Ellwood, B.B., 1988. Magnetic fabric of peridotite with intersecting petrofabric surfaces, Tinaquillo, Venezuela. *Phys. Earth Planet. Inter.,* 51:301–312.

MacLeod, C.J., and Rothery, D.A., 1992. Ridge axial segmentation in the Oman ophiolite: evidence from along-strike variations in the sheeted dyke complex. *In* Parson, L.M., Murton, B.J., and Browning, P. (Eds.), *Ophiolites and Their Modern Oceanic Analogues.* Geol. Soc. Spec. Publ. London, 60:39–64.

McCabe, C., Jackson, M., and Ellwood, B.B., 1985. Magnetic anisotropy in the Trenton Limestone: results of a new technique, anisotropy of anhysteretic susceptibility. *Geophys. Res. Lett.,* 12:333–336.

Nagata, T., 1961. *Rock Magnetism:* Tokyo (Maruzen).

Nicolas, A., Reuber, I., and Benn, K., 1988. A new magma chamber model based on structural studies in the Oman ophiolite. *Tectonophysics,* 151:87–105.

Nye, J.F., 1985. *Physical Properties of Crystals:* New York (Oxford Univ. Press).

Osborn, J.A., 1945. Demagnetizing factors of the general ellipsoid. *Phys. Rev.,* 67:351–357.

Pfleiderer, S., and Halls, H.C., 1990. Magnetic susceptibility anisotropy of rocks saturated with ferrofluid: a new method to study pore fabric? *Phys. Earth Planet. Inter.,* 65:158–164.

Richter, C., and van der Pluijm, B.A., 1994. Separation of paramagnetic and ferrimagnetic susceptibilities using low temperature magnetic susceptibilities and comparison with high field methods. *Phys. Earth Planet. Inter.,* 82:113–123.

Richter, C., van der Pluijm, B.A., and Housen, B.A., 1993. The quantification of crystallographic preferred orientation using magnetic anisotropy. *J. Struct. Geol.,* 15:113–116.

Rochette, P., and Fillion, G., 1988. Identification of multicomponent anisotropies in rocks using various field and temperature values in a cryogenic magnetometer. *Phys. Earth Planet. Inter.,* 51:379–386.

Schmidt, P.W., 1993. Palaeomagnetic cleaning strategies. *Phys. Earth Planet. Inter.,* 76:169–178.

Schultz-Krutisch, T., and Heller, F., 1985. Measurement of magnetic susceptibility in Buntsandstein deposits from Southern Germany. *J. Geophys.,* 57:51–58.

Smith, G.M., and Banerjee, S.K., 1985. Magnetic properties of plutonic rocks from the central North Atlantic Ocean. *In* Bougault, H., Cande, S.C., et al., *Init. Repts. DSDP,* 82: Washington (U.S. Govt. Printing Office), 377–383.

Stephenson, A., 1994. Distribution anisotropy: two simple models for magnetic lineation and foliation. *Phys. Earth Planet. Inter.,* 82:49–54.

Tarling, D.H., and Hrouda, F., 1993. *The Magnetic Anisotropy of Rocks:* London (Chapman and Hall).

Uyeda, S., Fuller, M.D., Belshé, J.C., and Girdler, R.W., 1963. Anisotropy of magnetic susceptibility of rocks and minerals. *J. Geophys. Res.,* 68:279–291.

Wagner, J.-J., Hedley, I.G., Steen, D., Tinkler, C., and Vuagnat, M., 1981. Magnetic anisotropy and fabric of some progressively deformed ophiolitic gabbros. *J. Geophys. Res.,* 86:307–315.

Wolff, J.A., Ellwood, B.B., and Sachs, S.D., 1989. Anisotropy of magnetic susceptibility in welded tuffs: application to a welded-tuff dyke in the Tertiary Trans-Pecos Texas volcanic province, USA. *Bull. Volcanol.,* 51:299–310.

Date of initial receipt: 1 August 1994
Date of acceptance: 12 December 1994
Ms 147SR-025